Optical Performance of a Wideband 28nm CMOS Double Bow-Tie Slot Antenna for Imaging Applications

van Berkel, S.L.; Malotaux, E.S.; Cavallo, D.; Spirito, M.; Neto, A.; Llombart, N.

DOI
10.1109/IRMMW-THz.2018.8510373

Publication date
2018

Document Version
Accepted author manuscript

Published in
43rd International Conference on Infrared Millimeter and Terahertz Waves, IRMMW-THz 2018

Optical Performance of a Wideband 28nm CMOS Double Bow-Tie Slot Antenna for Imaging Applications

S.L. van Berkel, E.S. Malotaux, D. Cavallo, M. Spirito, A. Neto, and N. LLombart
Department of Microelectronics, Delft University of Technology, Delft, The Netherlands

***Abstract*—The optical performance of a wideband double bow-tie slot antenna, implemented in 28nm CMOS technology, is evaluated. The antenna serves as a verification antenna for an uncooled single-pixel radiometer operating from 200 GHz to 600 GHz. The performance is evaluated in terms of radiometric pattern that is derived from the measured radiation patterns and simulated optical efficiency.**

I. Introduction and Background

Uncooled terahertz (THz) imagers suffer from high electronic noise that is introduced by the detectors. Detection is often performed incoherently since the use of coherent circuitry, such as mixers or (pre-)amplifiers, is still impractical for the fabrication of large, low-cost, low-power, imaging arrays. To compensate for the high electronic noise, one can resort to the use of active illumination [1] or try to exploit a large portion of the electromagnetic spectrum [2], so that a practical temperature sensitivity can still be achieved. This work focuses on developing a wideband fully passive THz radiometer that is integrated in a CMOS technology to enable low-cost imaging applications.

A typical problem that arises in developing CMOS antennas is the excitation of surface waves in the bulk silicon of the technology. This results typically in inefficient and narrow band operation. A solution to avoid the excitation of surface waves is to utilize dielectric lenses. An additional argument to use dielectric lenses is that a large Focal Plane Array (FPA) can be integrated in the CMOS chip that, when placed in the focal plane of the dielectric lens, will create a staring array that enables imaging applications.

Efficient planar wideband antenna solutions that are suitable for CMOS integration and that will illuminate a dielectric lens efficiently are leaky-lens antennas [3] and double-slot type antennas [4]. Both antenna solutions can operate efficiently over a 1:3 relative bandwidth thanks to a slightly enhanced leaky-wave radiation due to a small SiO2 layer of 5 µm separating the antenna layer from the low-resistive silicon of the technology. A schematic of the 28nm CMOS stratification is shown in Fig. 1(a).

This paper presents the optical performance of a fully passive single pixel radiometer fabricated in 28nm CMOS technology [5,6] in terms of its spectral radiation patterns and effective radiometric pattern [2]. The radiometer presented in [5,6] is a double bow-tie slot antenna [3] connected to a PN-junction diode. Since a radiometer integrates power incoherently over the full operational bandwidth, no spectral information can be resolved at the output of the detector. For verification purposes, a standalone antenna, without detector, is fabricated next to the pixel that exhibits similar performance. The verification antenna is shown in Fig. 1(b). The antenna can be accessed via a WR3 landing probe, such that the pixel's spectral performance can be analyzed using a vector network analyzer and WR2-2 extenders.

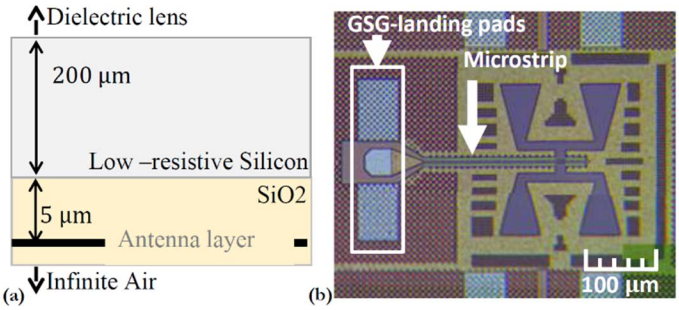

Fig. 1. (a) Schematic of the CMOS stratification. The antenna layer is separated by 5 µm of SiO2 from the low-resistive silicon that is thinned down to 200 µm. The chip is glued to a silicon dielectric lens; (b) Verification antenna of the radiometer. The double bow-tie slot antenna can be accessed with a landing probe on the GSG-landing pads, that are connected to the antenna with a microstrip transmission line.

Important figures of merit of a radiometric imager are temperature sensitivity and resolution. To analyze both parameters simultaneously in a qualitative manner, a suitable representation for the received power, P_a, in an uncooled radiometer can be written as (1) [2]:

$$P_a = \frac{k_B}{4\pi}\int T_S(\Omega)G_{\text{eff}}(\Omega)\mathrm{d}\Omega \qquad (1)$$

where k_B is Boltzmann's constant, T_S is the temperature of the blackbody source to be imaged and $G_{\text{eff}}(\Omega)$ is the effective radiometric pattern, which represents the detector's incoherent integration of power over frequency:

$$G_{\text{eff}}(\Omega) = \int_{200\text{ GHz}}^{600\text{ GHz}} \eta_{\text{opt}}(f)D(f,\Omega)\mathrm{d}f \ . \qquad (2)$$

In (2), $\eta_{\text{opt}}(f)$ is the optical efficiency and $D(f,\Omega)$ is the spectral directivity. In such definition, the effective radiometric pattern provides insight on how efficiently a radiometer is integrating power angularly. In order to evaluate the spectral components in (2), the verification antenna shown in Fig. 1(b) is fabricated and evaluated in terms of spectral performance.

II. Results

The CMOS chip is packaged in a quasi-optical system that defines the radiometer. The chip is glued to a silicon elliptical lens that is provided with an anti-reflection coating to reduce the reflections occurring at the silicon-air interface. The elliptical lens illuminates a hyperbolic lens via two flat gold mirrors. The hyperbolic lens creates a focus point in an image plane positioned 20 cm from the radiometer. The two flat

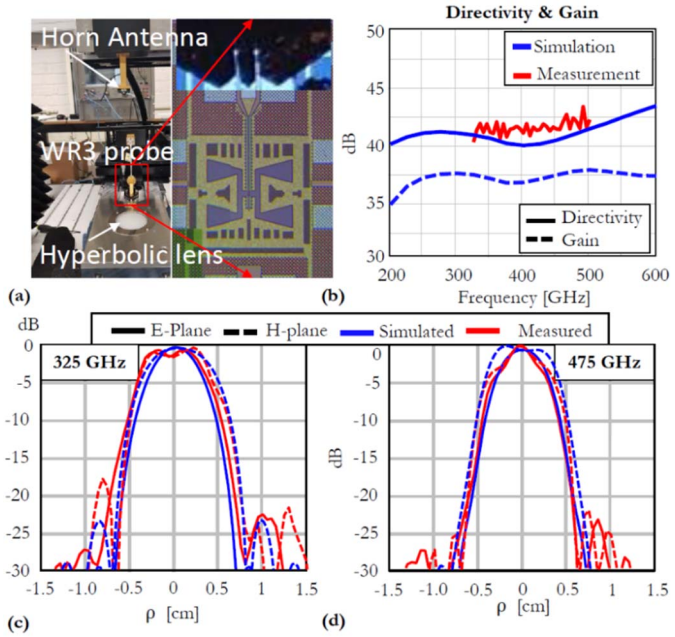

Fig. 2. (a) Measurement setup with a horn antenna placed in the image plane of a double bow-tie slot antenna; (b) simulated and measured directivity and simulated gain; simulated and measured radiation patterns at (c) 325 GHz and (d) 475 GHz.

mirrors are used to be able to access the CMOS chip with a landing probe while simultaneously a planar scan in the image plane can be performed.

The near-field directivity [7] is measured using a WR3 landing probe and the planar scan in the image plane is performed by a WR2.2 horn antenna. The measurement setup is shown in Fig 2(a). A zoom-in shows the WR3 landing probe that is landed on the GSG-landing pads that are connected to the antenna with a microstrip line. The horn antenna is positioned 20 cm above the hyperbolic lens and performs a 3 cm x 3 cm planar scan. The antenna is measured in the WR2.2 band from 325 GHz to 500 GHz. The measured and simulated directivity is shown in Fig. 2(b) and show a good agreement. The small oscillations in the directivity are attributed to the multiple reflections inside the radiometer. The simulated gain is also shown in Fig. 2(b). The gain is nearly constant over the full frequency band of the radiometer from 200 GHz to 600 GHz. The average optical efficiency over frequency of the radiometer is 41%.

The normalized spectral radiation patterns, measured at 325 GHz and 475 GHz, are shown in Fig. 2(c) and (d) respectively. Important to note is the highly frequency independent beams due to flat near-field gain curve.

The flat characteristic of the gain curve implies that the radiometer integrates power efficiently over the full operational bandwidth, illustrating the benefit of using wideband antennas in THz radiometry. The temperature sensitivity of the radiometer will be linearly proportional to received power [2] and thus a flat near-field gain in (2) is desired. The measurement setup is planned for calibration. After calibration, the optical efficiency and gain can be measured such that the effective radiometric pattern can be evaluated in absolute terms.

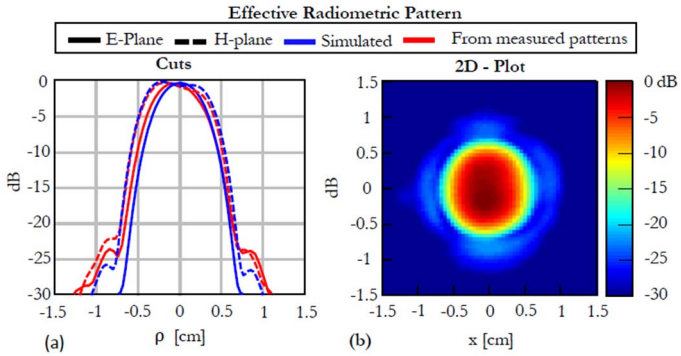

Fig. 3. Effective radiometric pattern [2], defined with eq. (2), representing the radiometer's incoherent integration of power over frequency. The radiometric pattern has a −10dB spot-size of 1 cm in diameter: (a) cuts in the E-plane and H-plane and (b) two-dimensional (2D) plot.

In this contribution, the radiometric pattern (2) is evaluated by using the simulated optical efficiency and measured radiation patterns. In Fig. 2(a) and (b) the E-/H-plane cuts and the 2D-scan of the effective radiometric pattern are respectively shown. The effective radiometric pattern is symmetric and features a −3 dB spot-size in the image plane of 0.8 cm in diameter.

ACKNOWLEDGMENTS

This research is supported by the Dutch Technology Foundation STW (TiCAM, 13325), which is part of the Netherlands Organization for Scientific Research (NWO), and which is partly funded by the Ministry of Economic Affairs. N. Llombart would like to thank the European Research Council for the starting grant LAA-THz-CC (639749). The work of A. Neto was supported by European Research Council Consolidator Grant AAATSI (278794). The authors would like to thank NXP Semiconductors for the technology access.

REFERENCES

[1] R. Hadi et. al., "A 1 k-Pixel Video Camera for 0.7-1.1 Terahertz Imaging Applications in 65-nm CMOS", *IEEE J. Solid-State Circuits,* vol. 47, no. 12, pp. 2999-3012, Dec. 2012.

[2] S. L. van Berkel, O. Yurduseven, A. Freni, A. Neto and N. Llombart, "THz imaging using uncooled wideband direct detection focal plane arrays," *IEEE Trans. THz Sci. Technol.*, vol. 7, no. 5, pp. 481-492, Sep. 2017.

[3]. O. Yurduseven, D. Cavallo, A. Neto, G. Carluccio, and M. Albani, "Parametric analysis of extended hemispherical dielectric lenses fed by a broadband connected array of leaky-wave slots," *IET Microw. Antennas Propag.,* vol. 9, no. 7, pp. 611-617, May 2015.

[4] A. J. Alazemi, H. H. Yang, and G. M. Rebeiz, "Double bow-tie slot antennas for wideband millimeter-wave and terahertz applications," *IEEE THz Sci. Technol.*, vol. 6, no. 5, pp. 682-689, Sep. 2016.

[5] S. L. van Berkel, E. S. Malotaux, D. Cavallo, M. Spirito, A. Neto and N. Llombart, "Wideband single pixel radiometer in CMOS," *42nd Int. Conf. Infrared, Millimeter and THz Waves*, Cancun, Mexico, 27 Aug.-1 Sept. 2017.

[6] S.L. van Berkel, et.al., "Wideband Single Pixel Radiometer in 28nm CMOS Technology for Low-Cost Imaging Applications," *12th Eur. Conf. Antennas Propag.,* London, U.K., Apr. 9-13, 2018.

[7] R. Hansen, "Focal region characteristics of focused array antennas," IEEE Trans. Antennas Propag., vol. 33, no. 12, pp. 1328–1337, 1985.